Current Status on Radiation Modeling for the Hayabusa Re-entry

Michael W. Winter
University Affiliated Research Center UARC, UC Santa Cruz

Ryan D. McDaniel, Yih-Kanq Chen, Yen Liu
NASA Ames Research Center, Moffett Field, CA 94035

David Saunders
ERC, Incorporated

Acknowledgments

Thanks to George Raiche , Aga Goodsell, and Jay Grinstead (NASA Ames) for support of the current work, Peter Jenniskens (SETI) , Jim Albers (SETI), Alan Cassell (ERC Inc.), Dinesh Prabhu (ERC, Inc.), Nicholas Clinton (UARC), Jeffrey Myers (UARC), and Mike Olsen (NASA Ames) for supporting with data, information, and help, Jonathan Snively (Embry-Riddle Aeronautical University), Mike Taylor (Utah State University), David Buttsworth, and Richard Morgan (University of Southern Queensland) for providing preliminary experimental data for a comparison with the predictions as well as everybody in the Aerothermodynamics Branch who supported in the one or the other way.
The present work was supported
by NASA Contract NAS2-03/44 to UARC, UC Santa Cruz, and
by NASA Contract NNA10DE12C to ERC Incorporated.

Current Status on Radiation Modeling for the Hayabusa Re-entry

Michael W. Winter
University Affiliated Research Center UARC, UC Santa Cruz

Ryan D. McDaniel, Yih-Kanq Chen, Yen Liu
NASA Ames Research Center, Moffett Field, CA 94035

David Saunders
ERC, Incorporated

Outline

- **Motivation and Methodology**
- **Numerical Procedures (DPLR, FIAT, NEQAIR)**
- **Application of the results to the Hayabusa observation mission**
- **Comparison with first experimental data**
- **Summary and Conclusions**

Motivation

- Re-entry speed 12 km/s
  → second fastest re-entry of an artificial object
  → Peak heat flux of Hayabusa occurs at a velocity and altitude similar to Stardust
  → Important validation data for heat shield performance
- No TPS-related instrumentation aboard the capsule!
  → observation from outside.
- NASA Mission using modified DC-8
  flight altitude 12.5 km → no interference with clouds etc.
  but still absorption down to ~300nm in the ozone layer
- International Participants (USA, Japan, Germany, Australia) using 24 different set-ups covering the wavelength range from 300 nm to 1600 nm with spectral resolutions between 0.2 nm and 10 nm but no spatial resolution → **point source!**

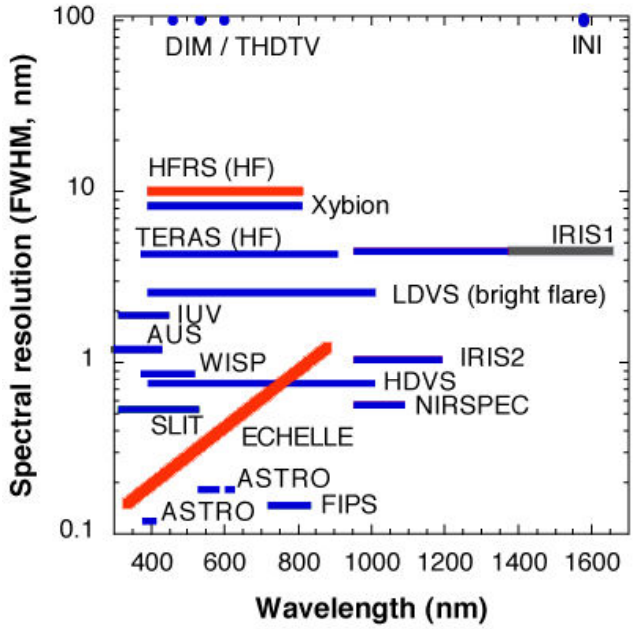

Radiation predictions are needed for:

- Pre-flight estimates of expected radiation levels
  → choice of appropriate calibration sources and signal strength
- Post-flight analysis for comparison with the experimental data
  → a baseline simulation is to be provided by NASA

Methodology

The current analysis essentially followed the methods applied to the Stardust Observation (2006) by Yen Liu et al.[#] However, thermal and plasma radiation were computed separately. The following tasks were performed:

- Simulate the flow field around the capsule at selected trajectory points
  → species densities and temperatures in the flow field + radiation equilibrium wall temperatures
- Post-process the DPLR data with the material response code FIAT
  → adapted surface temperatures
- Extract lines of sight through the plasma using view angles from trajectory simulation
- Compute spectral radiance along these lines of sight with NEQAIR
- Integrate over all lines of sight to determine total plasma radiation
- Determine effective surface areas for each axial position on the heat shield
- Compute Planck radiation according to the surface temperature distribution
- Propagate the sum of plasma and thermal radiation using the corresponding solid angle at the given trajectory point
  → incident total radiant power
- Convert received total radiant power into incident irradiance at the DC8 position.

[#] Yen Liu, Dinesh Prabhu, Kerry A. Trumble, David Saunders, and Peter Jenniskens, *Radiation Modeling for the Reentry of the Stardust Sample Return Capsule*, Journal of Spacecrafts and Rockets, Vol. 47, No. 5, September–October 2010.

Flow Field Simulation with DPLR

DPLR - Data-Parallel Line Relaxation code:

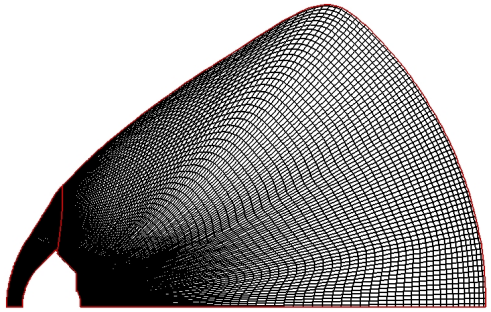

•. Standard 3-D nonequilibrium Navier-Stokes flow solver used by NASA for high-speed flow computations, validated over a wide spectrum of flight and ground-based experimental simulations.

- Surface fully catalytic and in radiative equilibrium with $\varepsilon = 0.89$.
- Solutions run fully laminar or fully turbulent.
- Finite-rate chemistry with 11-species air chemistry model (Park 1990 : N_2, O_2, NO, NO+, N_2+, O_2+, N, O, N+, O+, e,) and thermal nonequilibrium with two-temperature model (T and T_v).
- Hayabusa: Axisymmetric solution, roughness induced transition predicted (Re_{kk}=100 at 58km)

→ both laminar and turbulent solutions generated for all altitudes.

FIAT - Fully Implicit Ablation and Thermal Response Program:

1-D time-accurate solution of thermal diffusion with surface ablation and internal pyrolysis

- Multilayer material stack TPS, adhesive, insulation, structure, air gap, etc.
- Planar, cylindrical, or spherical geometry
- For Hayabusa carbon phenolic was used as TPS material

NEQAIR - Nonequilibrium Air Radiation line-by-line radiation code:

- Emission and absorption of atoms (N, O, H, C, He) and molecules (N_2, N_2^+, NO, O_2, H_2, CO, C_2, CN).
- Features: Bound-free and free-free continuum; Doppler, Stark, resonance, and collisional broadening plus additional instrument broadening in form of Voigt profiles;
- Radiative transport is computed along a line-of-sight as a series of one-dimensional cells
- For Hayabusa: O, N, N_2, N_2^+, and O_2 due to the wavelength range (ablation products not available in DPLR).

Trajectory information

- From Hayabusa to DC-8: elevation and azimuth angles
- No angle of attack and rotational symmetry → only azimuth important
  (azimuth: angle between vector to observer and flight path vector)

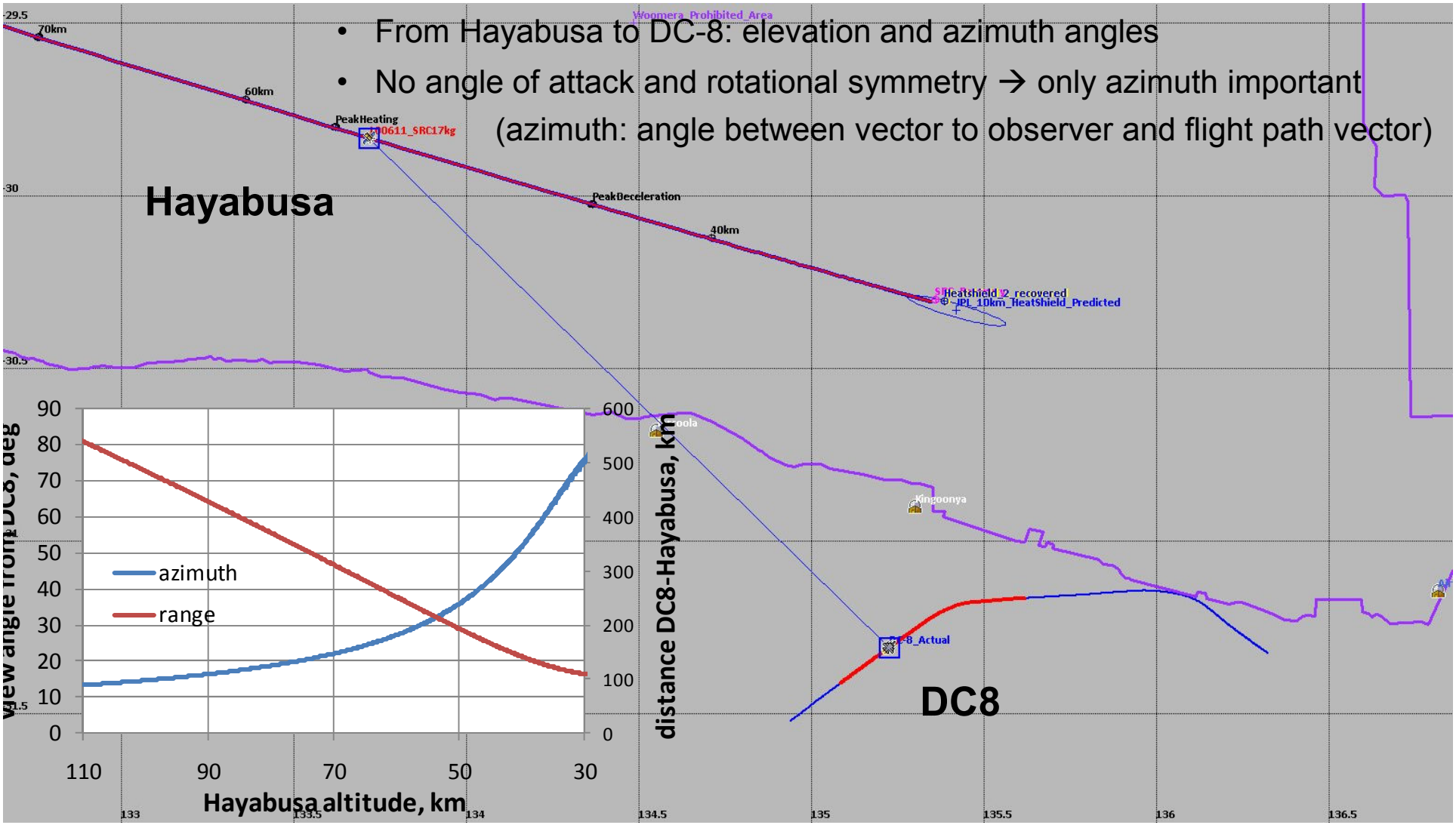

Trajectory information

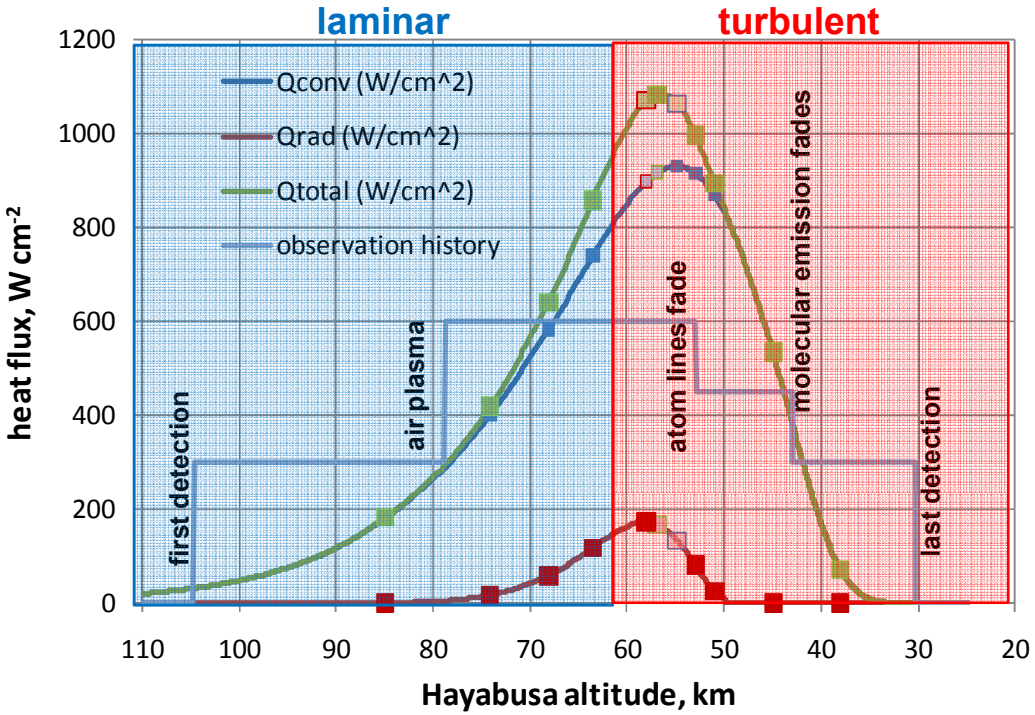

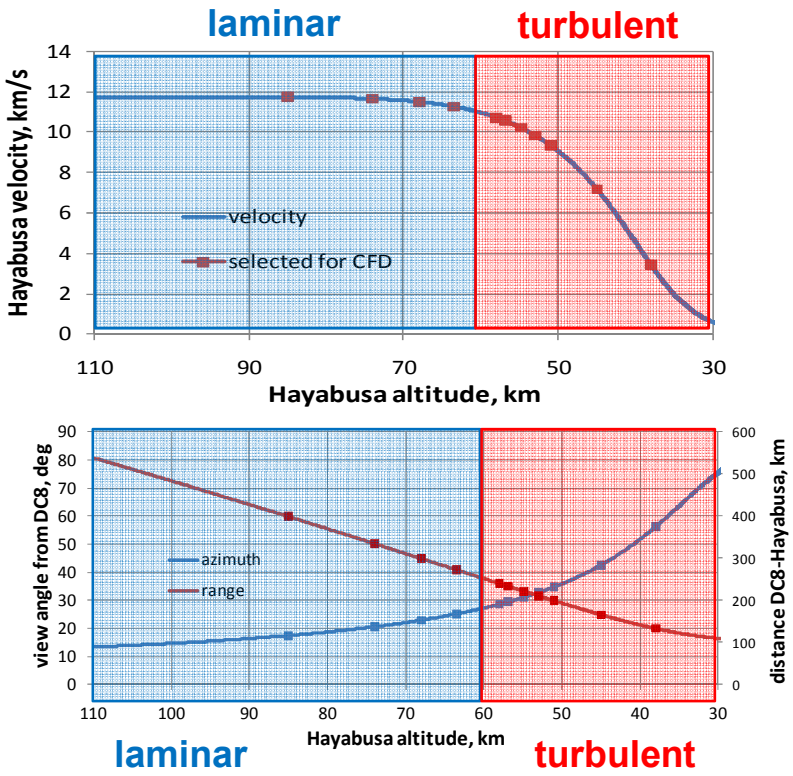

- Pre-flight, CFD solutions for radiative, convective, and total peak heating were computed.
- Post-flight, these solutions were recomputed with updated trajectory information. Four trajectory point on each side of peak heating were added with emphasis on covering the range where spectroscopic data was measured.
- The maximum altitude for CFD was reached at 74km altitude where the limiting Knudsen number of 0.01 for continuum flows was reached. A computation at 85km did not converge.

DPLR results

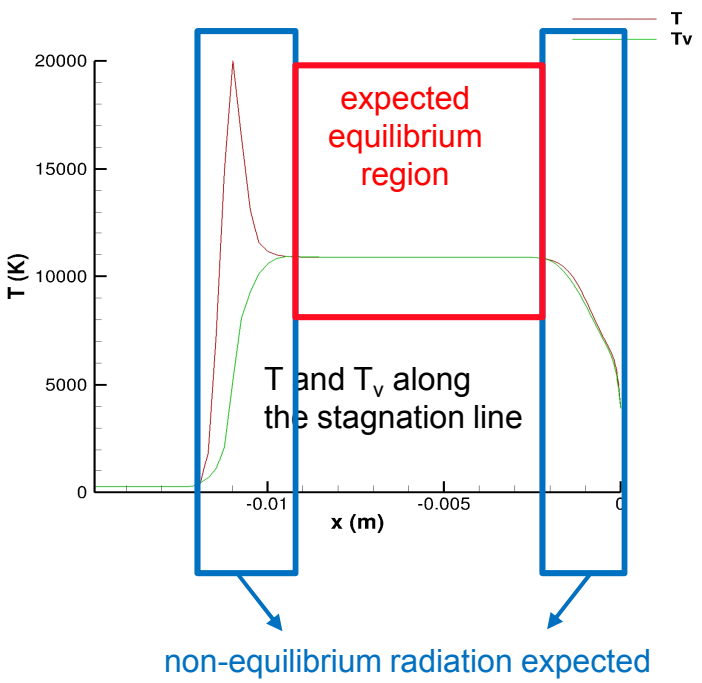

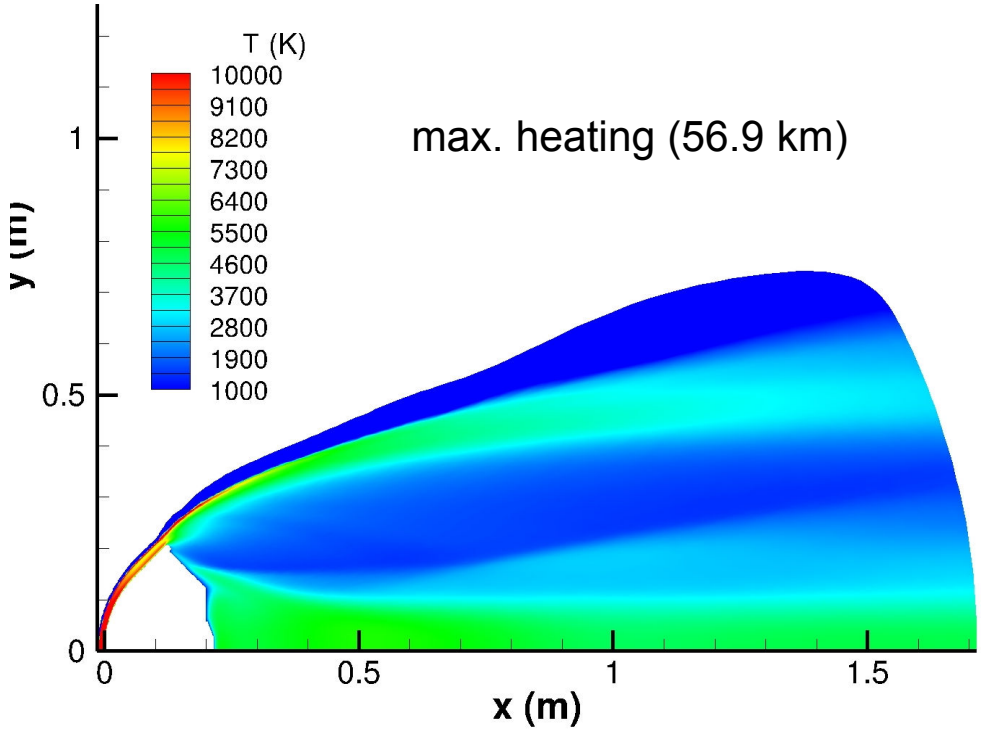

- DPLR → nonequilibrium flow field data
  → radiation equilibrium surface temperatures
- Temperatures along the stagnation line show a distinct plateau
  → indicates the equilibrium region behind the shock.
- For the loads on the heat shield, only the forebody solution is necessary, but lines of sight under a given view angle require the wake as well.

DPLR results

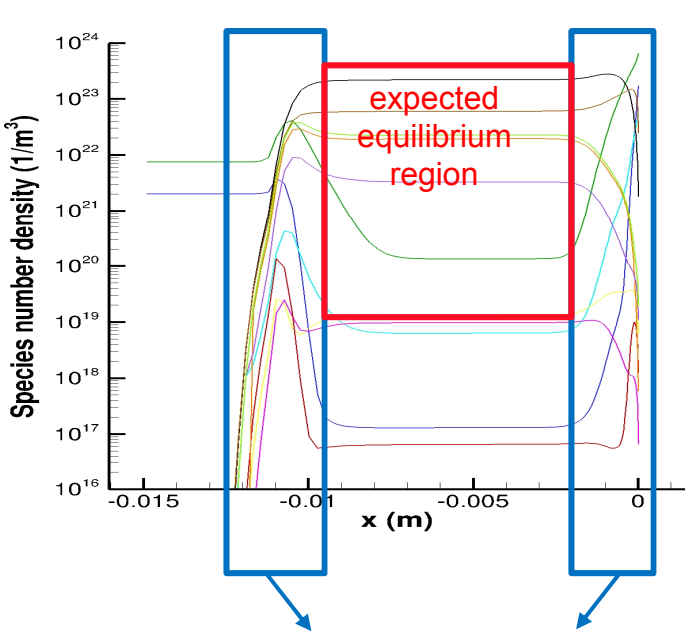

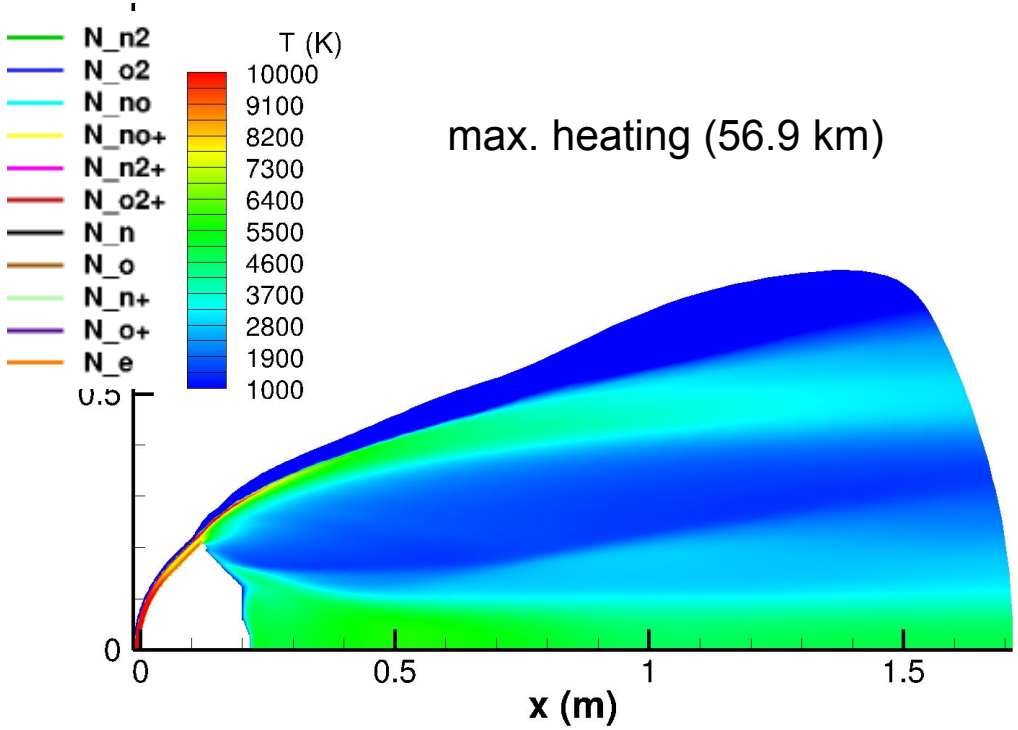

max. heating (56.9 km)

- DPLR → nonequilibrium flow field data
  → radiation equilibrium surface temperatures
- Temperatures along the stagnation line show a distinct plateau
  → indicates the equilibrium region behind the shock.
- For the loads on the heat shield, only the forebody solution is necessary, but lines of sight under a given view angle require the wake as well.

Extraction of lines of sight

- Generate 3d flow field by rotating the 2d flow solution.
- Create a uniform 2d orthogonal grid perpendicular to the view angle vector behind the flow field
- Generate lines of sight for each grid element: determine intersections with flow field outer boundary and capsule surface, and eliminate “empty” line segments.

- Due to the large distance to the observer, parallel lines are sufficient.
- lines are cut off in the wake at a specified distance from the body (0.1 x capsule length).

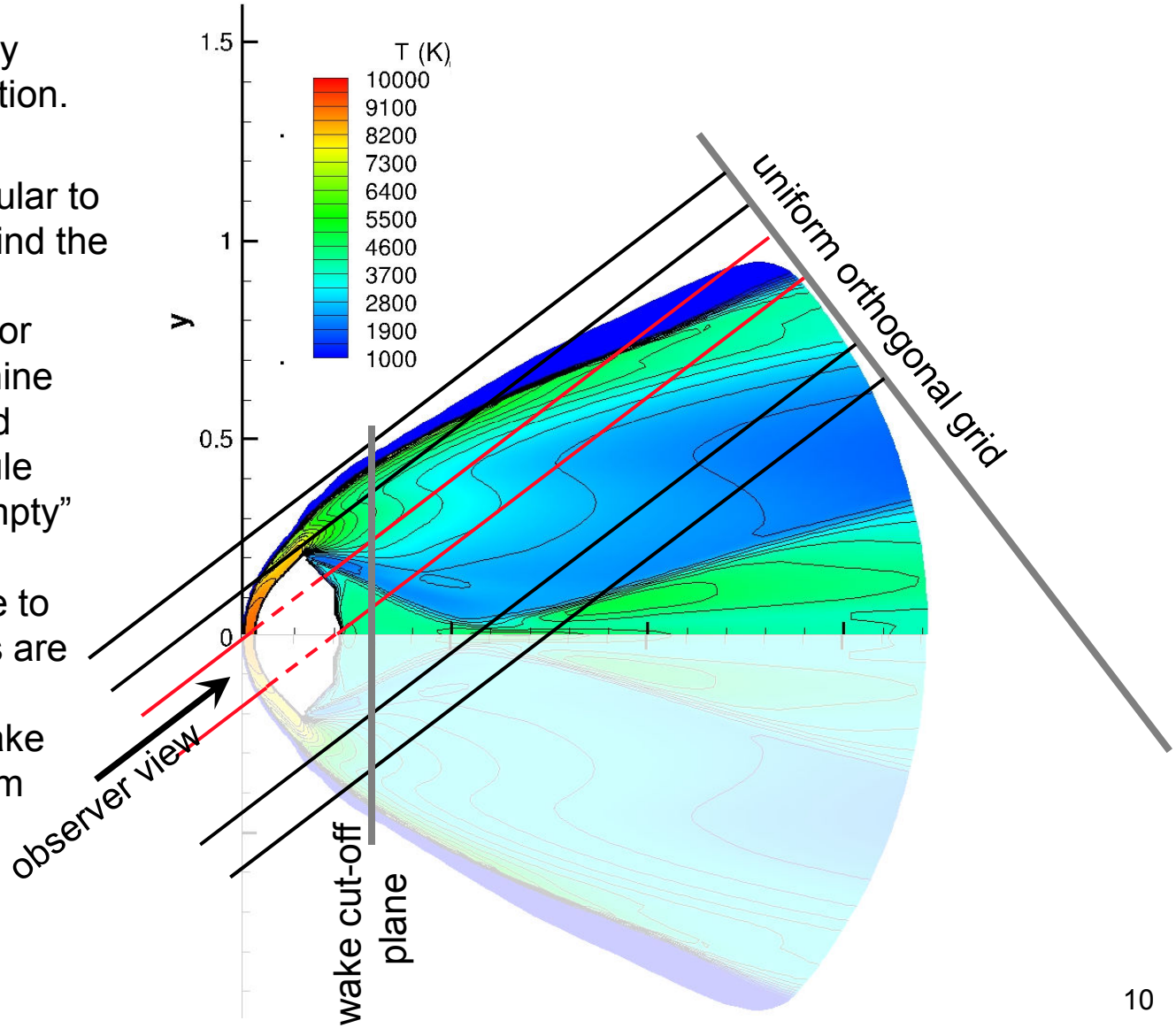

Extraction of lines of sight

- Generate 3d flow field by rotating the 2d flow solution.
- Create a uniform 2d orthogonal grid perpendicular to the view angle vector behind the flow field
- Generate lines of sight for each grid element: determine intersections with flow field outer boundary and capsule surface, and eliminate “empty” line segments.

- Due to the large distance to the observer, parallel lines are sufficient.
- lines are cut off in the wake at a specified distance from the body (0.1 x capsule length).

Lines of sight for:

74km, 20.6 deg

53km, 32.7 deg

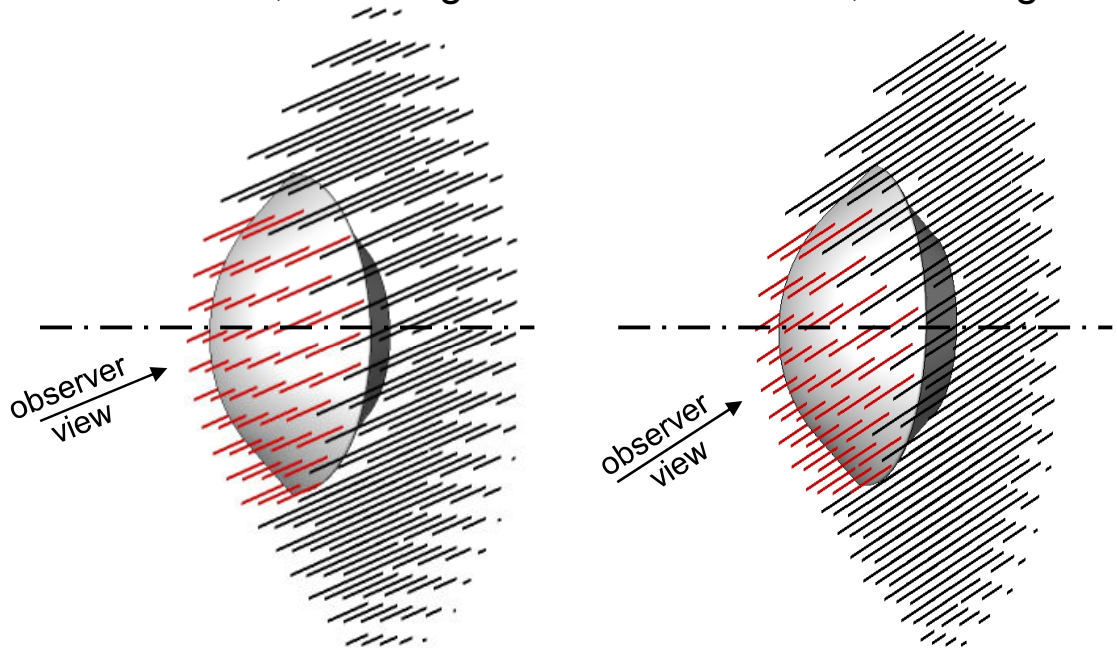

443-620 **inner** and 662-850 **outer** lines of sight were computed in the half space of the flow field for each trajectory point yielding a spatial resolution of ~1 cm^2.

Finally: Interpolate flow field data along these lines and convert to NEQAIR input.

NEQAIR Results

- NEQAIR runs were performed on all lines of sight for N, O, N_2 , O_2 ,and N_2^+ as the main radiating species in the wavelength range between 300nm and 1500nm
- Boltzmann excitation for equilibrium, QSS for non-equilibrium regions, both computed for all points.

- During initial runs, discrepancies in continuum emission were seen between Boltzmann and QSS
- NEQAIR results doubtful for deviations from equilibrium (in the current case, results more than 1 order of magnitude higher than with recent model from HyperRad)

→HyperRad procedure modified and bound-free continuum separately computed throughout the flow field.

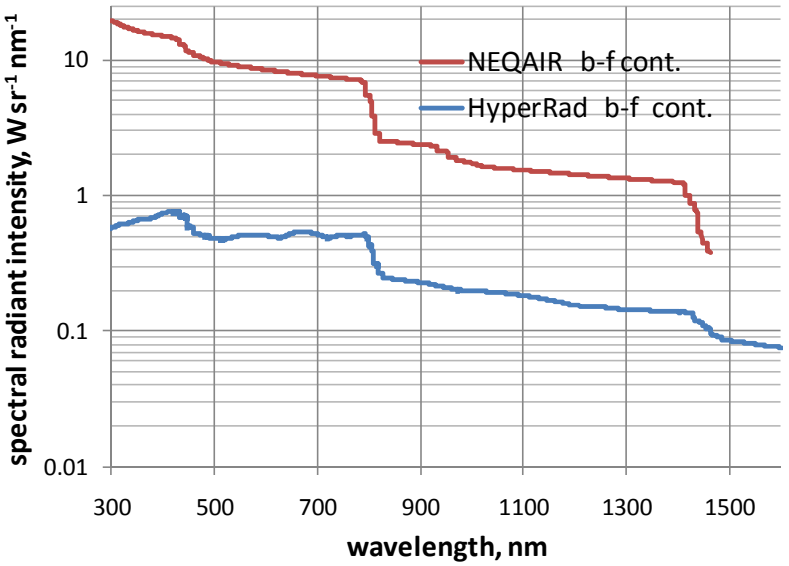

Winifred M. Huo, "Electron-Impact Excitation and Ionization in Air, " AIAA 2008-1207,
46th AIAA Aerospace Sciences Meeting and Exhibit, 7 - 10 January 2008, Reno, Nevada.

NEQAIR Results

- NEQAIR runs were performed on all lines of sight for N, O, N_2 and N_2^+ as the main radiating species in the wavelength range between 300nm and 1500nm
- Parameters: initial resolution 0.01nm, integrated to 0.2nm, and broadened to 0.5nm with Boltzmann excitation and Quasi-Steady State (QSS) assumption in separate runs.

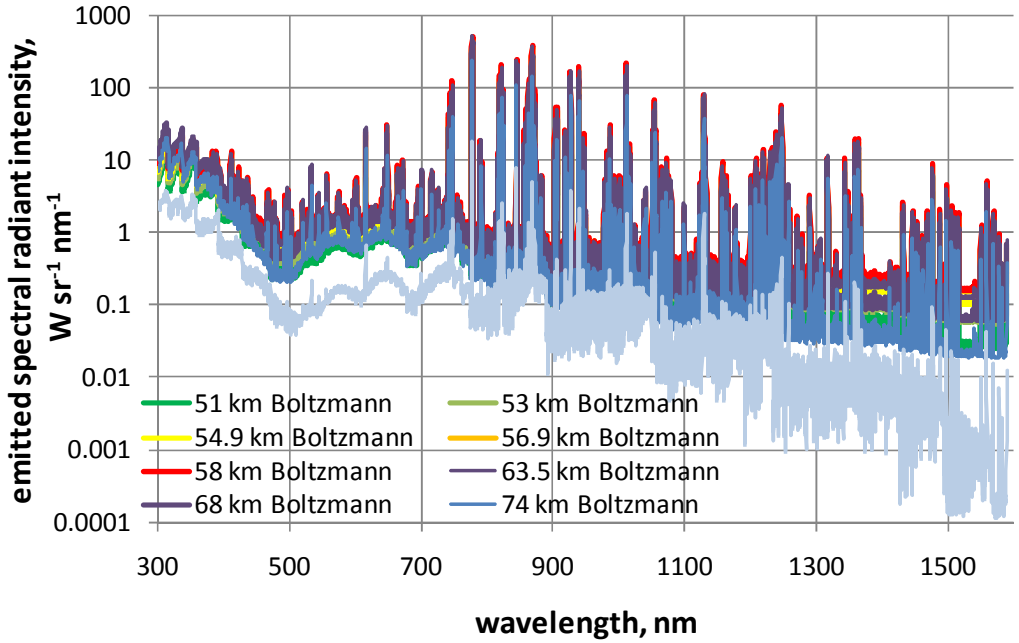

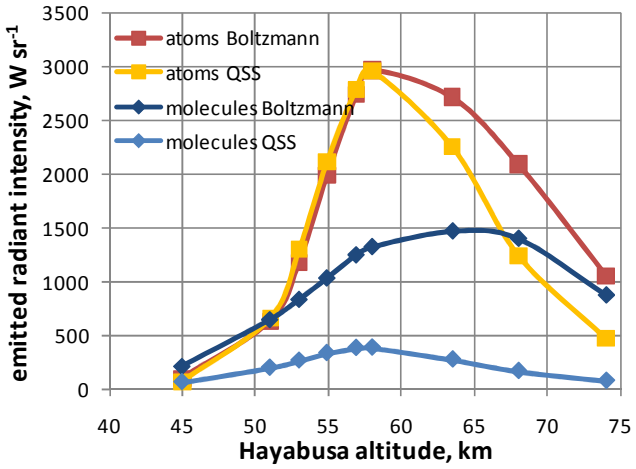

- Atom line emission: QSS < Boltzmann before peak heating, then about equal
- Molecule emission: QSS always lower (factors 3-8)

Thermal Radiation

- Thermal emission from the glowing heat shield a major part of the emitted radiation
- Computed as Planck radiation
  ε = 0.9 (charred carbon phenolic)

$$L_\lambda(T) = \varepsilon_\lambda \frac{2hc^2}{\lambda^5} \frac{1}{\exp\left(\frac{hc}{\lambda kT}\right) - 1}$$

- Point source measurement of total radiation
  → spectral radiance integrated over the surface

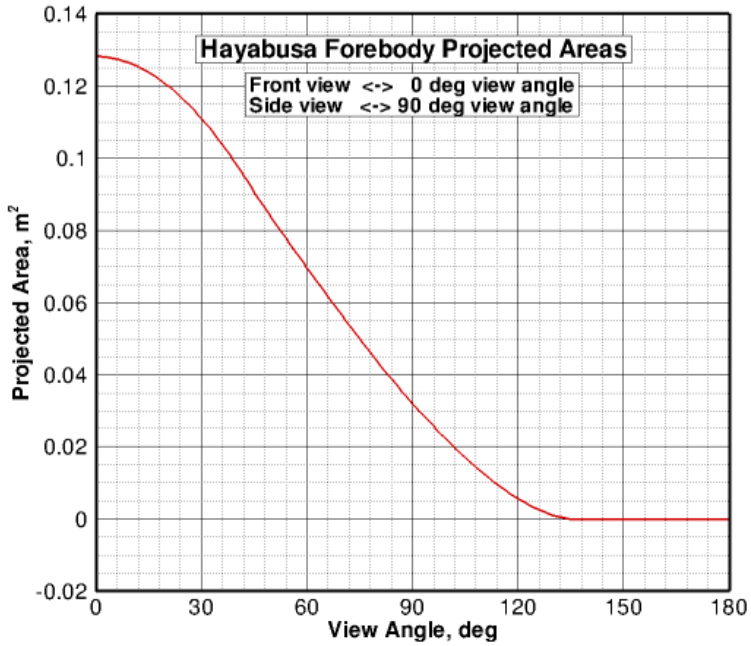

- As the capsule approaches the observer, the view angle to the surface changes continuously. Only the projected area can be used due to Lambert's Law.
- Computation of the projected area though a Fortran code (originally developed for the Stardust observation)

Effective (projected) surface areas

- To be able to account for temperature gradients, the projected areas were computed on the CFD surface grid for each circular ring of cells.
- The back shell was assumed to emit only negligible contributions to the total radiation.

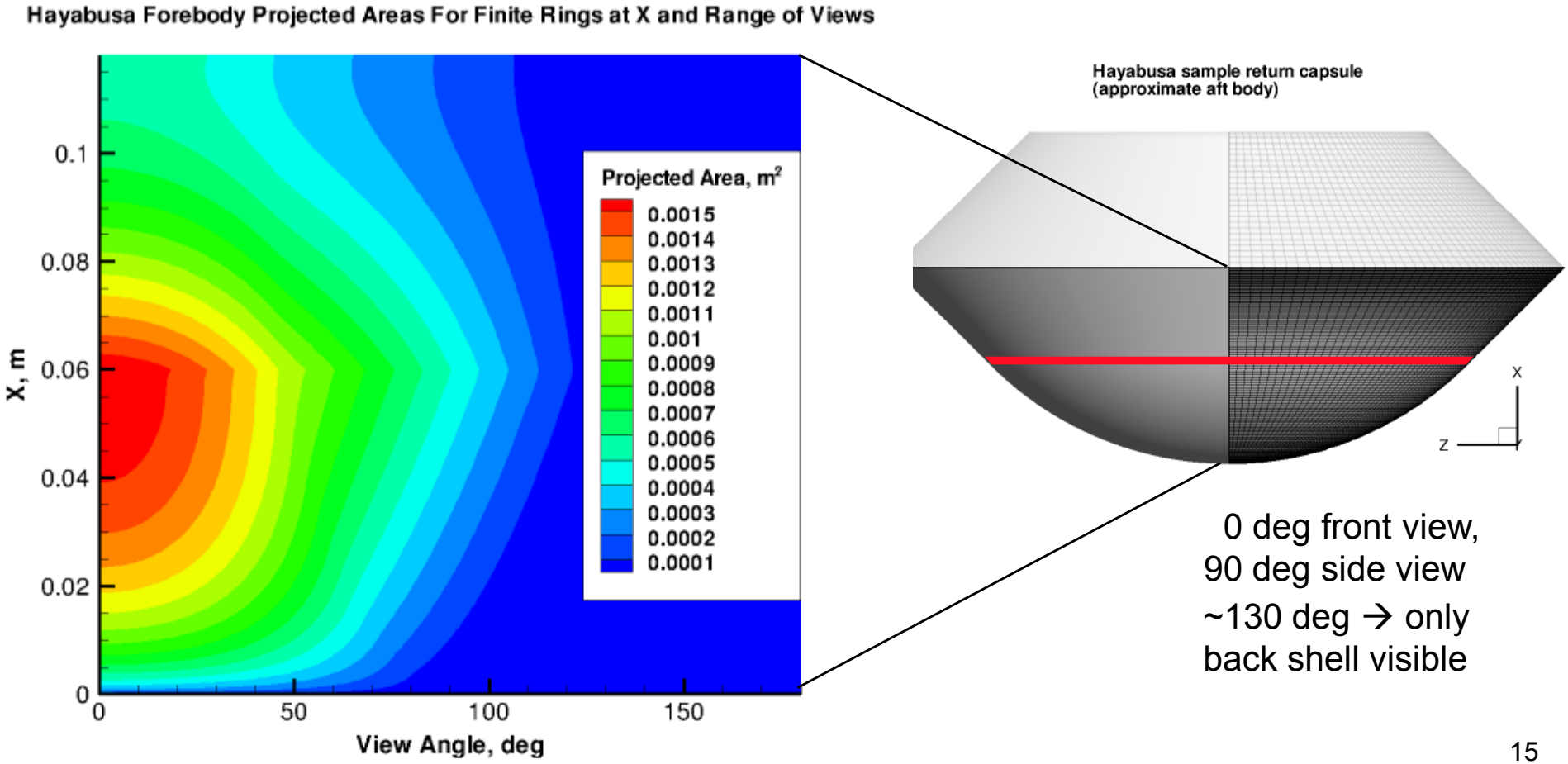

Surface Temperatures

- FIAT computations performed for 25 points along the surface resulting temperatures back-interpolated onto the 146 cells of the DPLR surface grid → radiation computation.
- Through material response, the temperature profiles show higher gradients across the surface for the laminar cases and flatten for the turbulent ones.
- Temperatures are significantly reduced by ~500K, except for the two trajectory points after convective peak heating which show only a moderate change.
- Turbulent heating increases the off-axis values and flattens out the profile.

FIAT and DPLR at peak heating

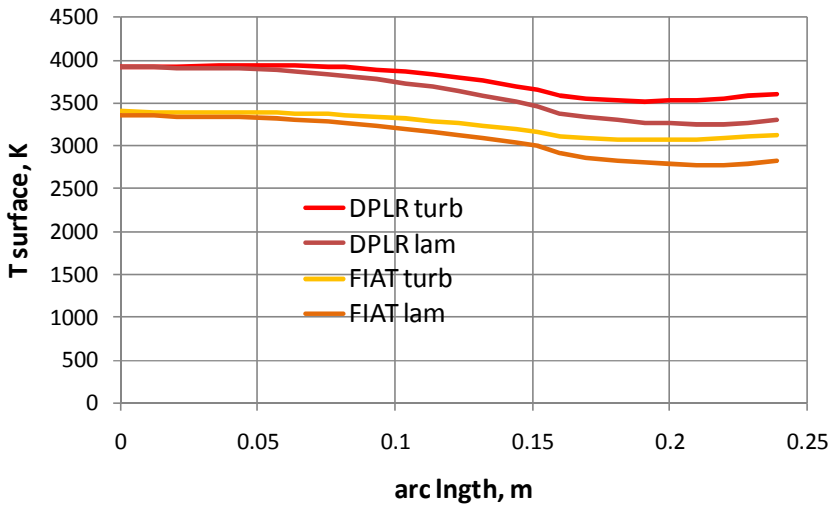

FIAT: material response

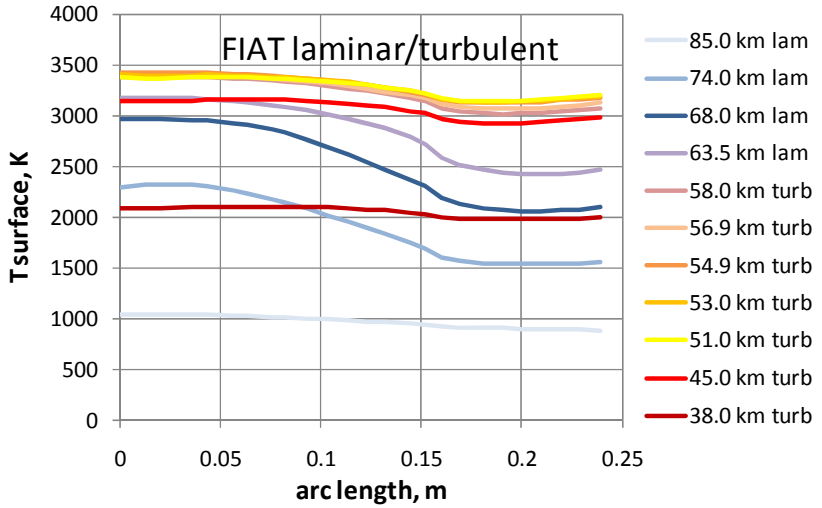

Radiation Transport

- Both plasma and surface radiation are computed in spectral radiance values (i.e. W m^{-2} nm^{-1} sr^{-1}).
- Along the trajectory, view angle and the solid angle vary with the distance.
- Instrument calibration to spectral irradiance (W m^{-2} nm^{-1})

→ predicted radiance converted to spectral radiant power (W/nm) through multiplication with $A_{emitting}$ (surface area or grid cell) and Ω and division by $A_{receiving}$

- Detected radiation partly absorbed by the atmosphere
  → τ computed with Modtran during pre-flight analysis.

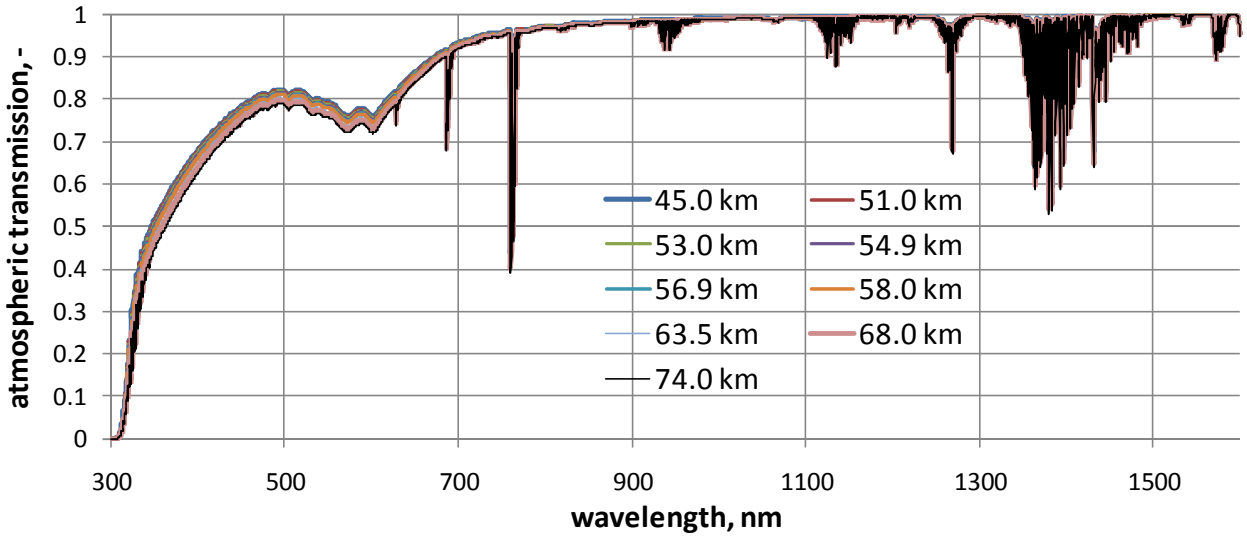

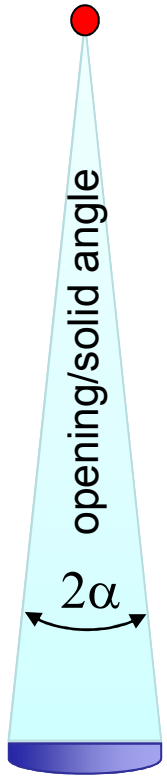

$$\Omega = 2\,\pi\,(1-\cos(\alpha))$$

Thermal Radiation

- Thermal radiation computed as Planck radiation. (ε = 0.9 for charred carbon phenolic)
- Spectral data converted from emitted spectral radiance to spectral irradiance received at the DC-8 position.

$$L_\lambda(T) = \varepsilon_\lambda \frac{2hc^2}{\lambda^5} \frac{1}{\exp\left(\frac{hc}{\lambda kT}\right) - 1}$$

- Significant increase in continuum radiation between 74 km and 68 km altitude
- Maximum of incident thermal radiation at 51 km altitude clearly after peak heating
- Turbulent flow increases the maximum of thermal radiation by ~40%

laminar solution

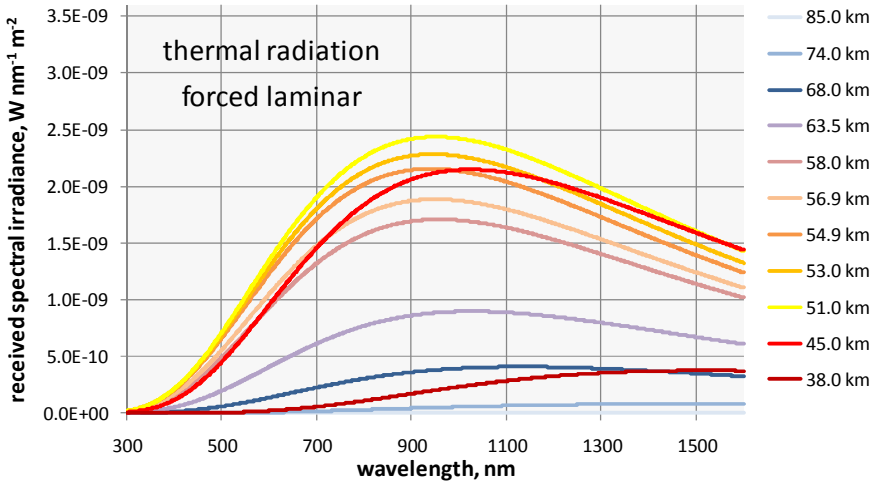

turbulent solution

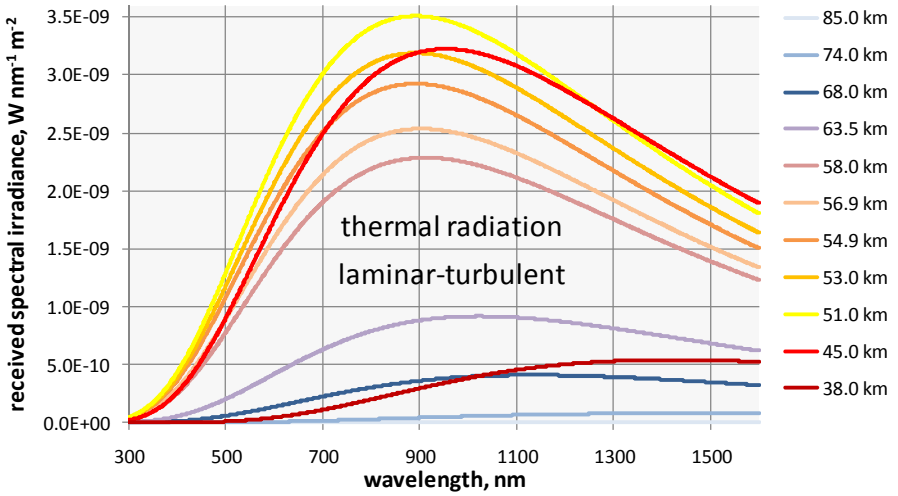

Incident Radiation

- The total incident radiation at the DC-8 position is given by the superposition of thermal and plasma emission.

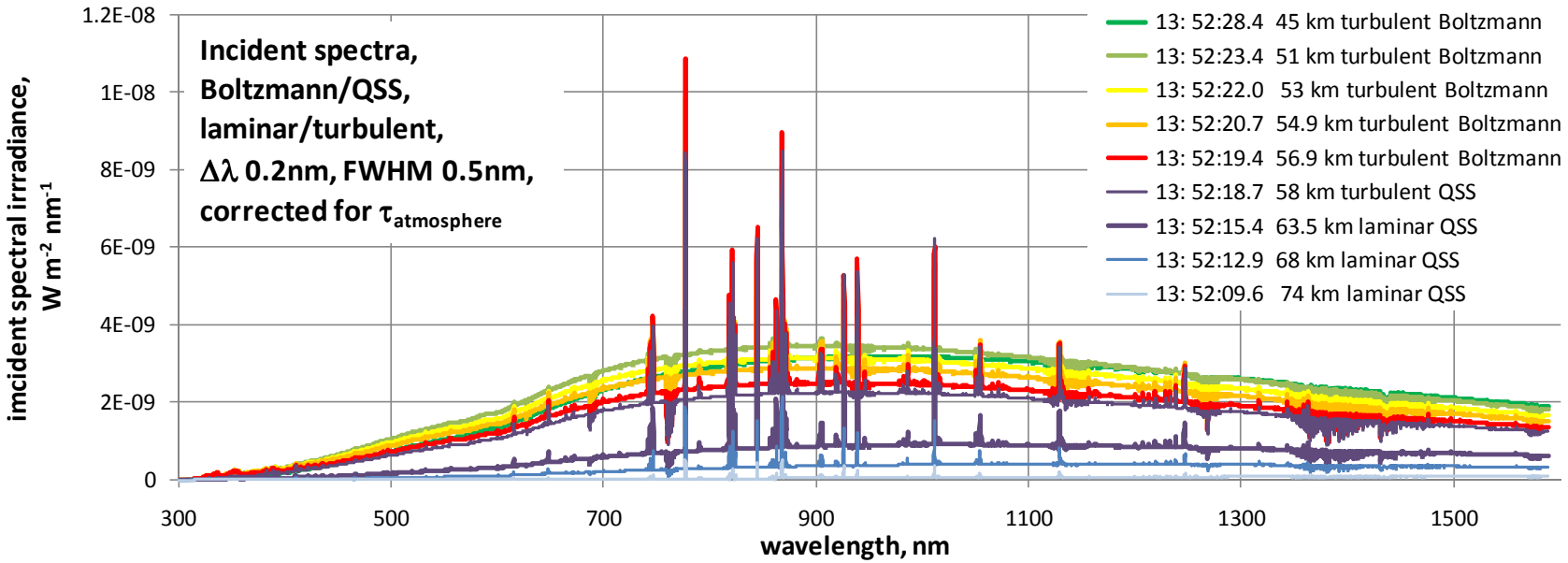

Combined thermal and plasma emission in high spectral resolution (HWFM 0.5nm)

Incident Radiation

- The total incident radiation at the DC-8 position is given by the superposition of thermal and plasma emission.
- The atom line emission of the plasma increases up to peak radiative heating and starts fading out after peak heating. After that point, the spectra are dominated by continuum emission. The molecular emission (mainly N_2^+), however, keeps increasing down to 51km altitude.

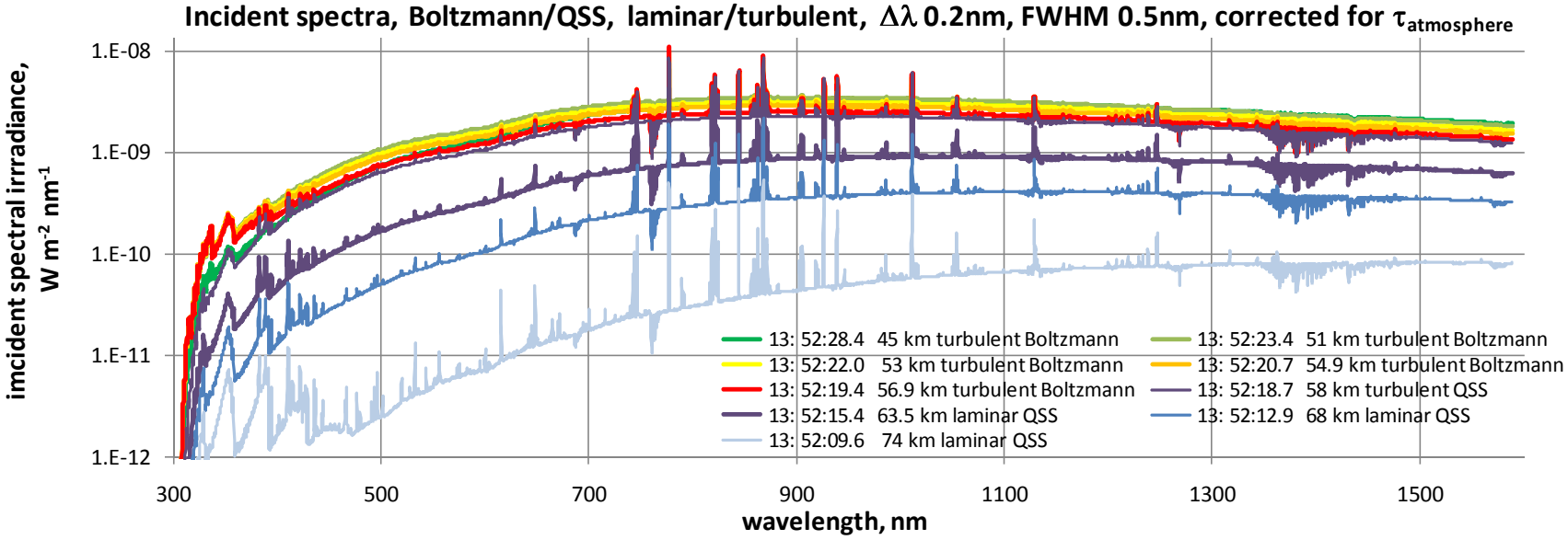

Combined thermal and plasma emission in high spectral resolution (HWFM 0.5nm)

Incident Radiation

- For a comparison with set-up without spectral resolution (e.g. tracking cameras), the incident irradiance can be integrated over the sensitive wavelength range (here done for 300nm to 1600nm)

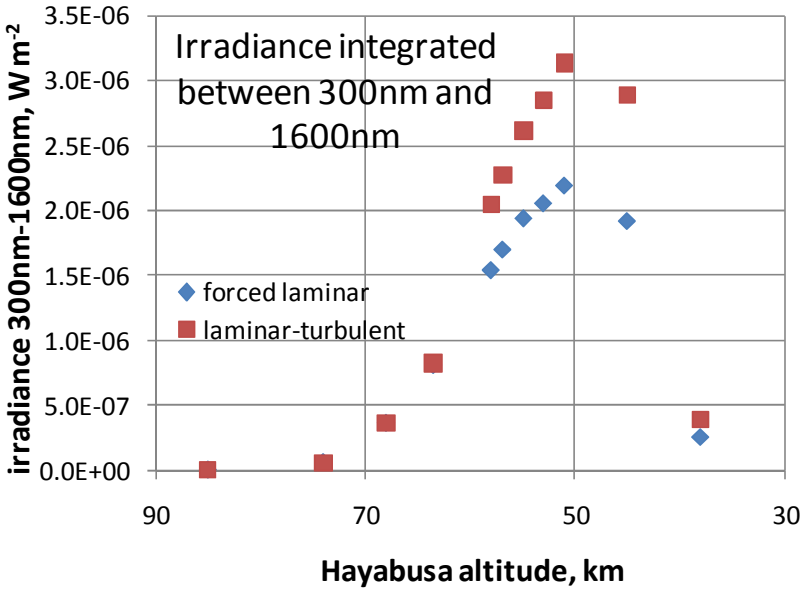

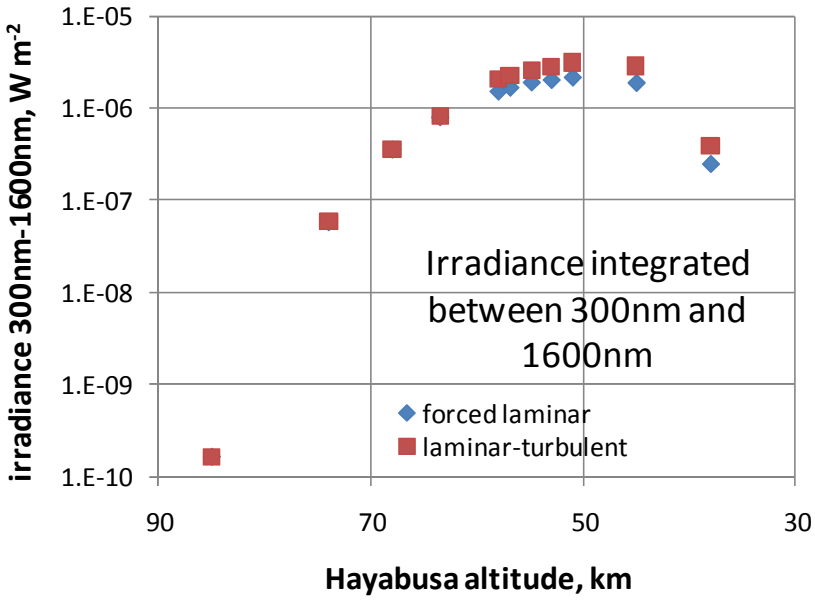

Preliminary Comparison with Experiment

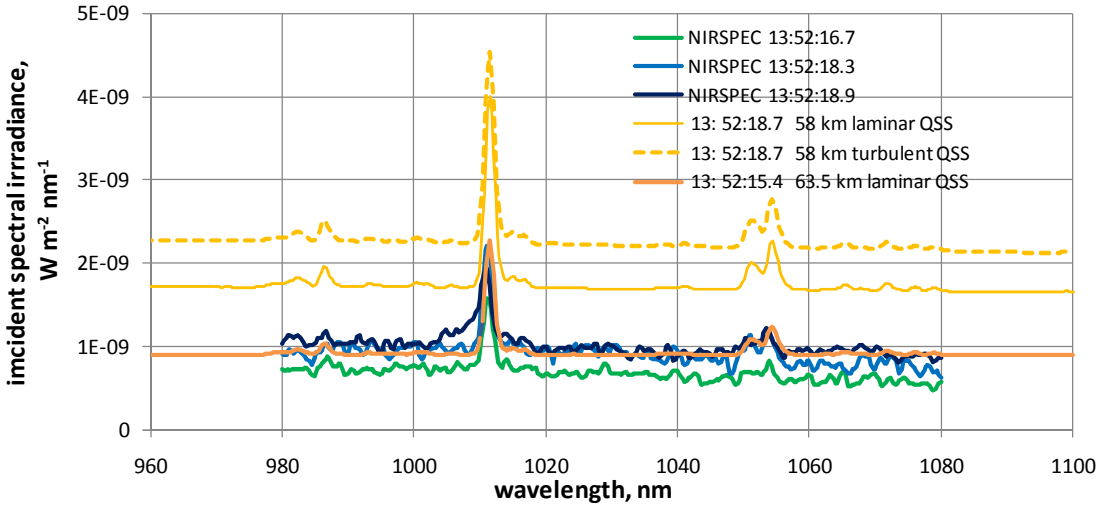

NIRSPEC (Utah State)

- Major emission from nitrogen lines and thermal continuum.
- Good qualitative agreement.
- Both plasma and thermal emission clearly weaker than the prediction.

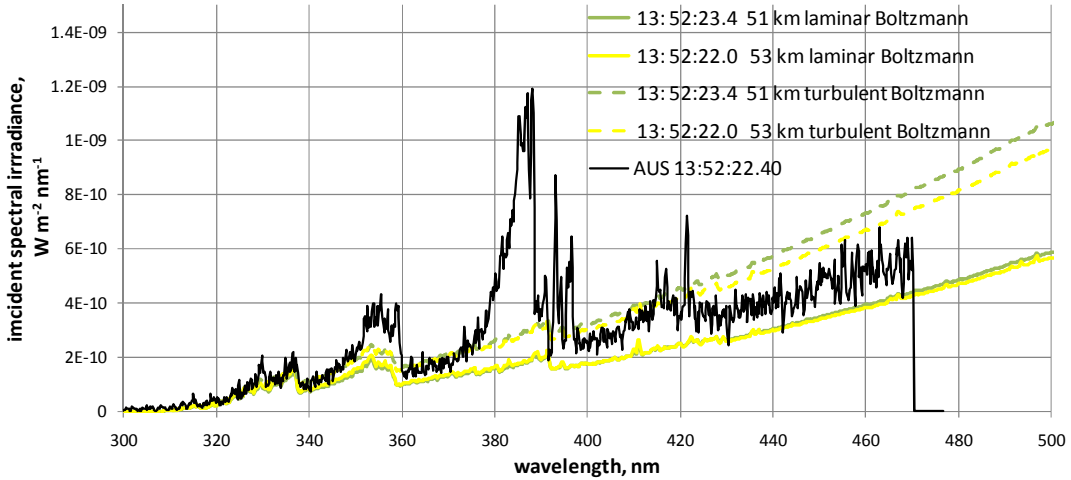

AUS (University of Queensland)

- Main emission from CN and thermal continuum, weak N2+ bands.
- CN is not yet included in the modeling but continuum in good agreement with laminar solution
  → no transition to turbulent or re-laminarization ?

David Buttsworth, Peter Jacobs, Daniel Potter, Neil Mudford, Mary D'Souza, Troy Eichmann, Richard Morgan, Peter Jenniskens, Tim McIntyre, Michael Jokic, Carolyn Jacobs, Ben Upcroft, Razmi Khan, Hadas Porat, and Andrew Neely, "Super-orbital Re-entry in Australia – laboratory measurement, simulation and flight observation," 28th International Symposium on Shock Waves, 17 - 22 July 2011, Manchester, UK.

How to proceed?

- A baseline solution for predicted radiation during the Hayabusa re-entry has been obtained from a combination of trajectory data, flow field solutions post-processed with a material response, line-by-line plasma simulation, and computation of Planck radiation. The resulting radiation has been propagated to the observer's position on the DC-8.
- A comparison with first experimental data showed good qualitative agreement in the NIR but weaker predicted values than measured. In the UV, the agreement of continuum radiation was very good for the assumption of a laminar flow. This indicates that no roughness induced transition to turbulence occurred but clear statements will rewuire more data along the trajectory.

- A new set of atomic line constants is in preparation to be implemented into *NEQAIR*. As soon as these data are available, the results will be recomputed.

- A re-computation of the flow field with surface blowing and ablation product chemistry seems desirable to be able to compare with the major molecular radiators in the experimental data (i.e. CN) and other ablation products (e.g. H).
DPLR is able to handle surface blowing but the inclusion of ablation chemistry in the flow field has yet to be finally implemented.

Thank you!
Happy to answer

Questions ?

Trajectory information

Selected trajectory points:

point	UTC	altitude	lam/turb	view angle	range	$T_{surf,stag,FIAT}$	
1	13:52:03.8	85 km	lam	17.5 deg	398.9 km	1050 K	(not converged)
2	13: 52:09.6	74 km	lam	20.6 deg	334.8 km	2296 K	
3	13: 52:12.9	68 km	lam	22.9 deg	299.3 km	2961 K	
4	13: 52:15.4	63.5 km	lam	25.2 deg	272.5 km	3178 K	
5	13: 52:18.7	58 km	turb	28.6 deg	239.9 km	3381 K	$q_{rad,max}$
6	13:52:19.4	56.9 km	turb	29.4 deg	233.3 km	3401 K	**$q_{tot,max}$**
7	13:52:20.7	54.9 km	turb	31.0 deg	221.5 km	3423 K	$q_{conv,max}$
8	13:52:22.0	53 km	turb	32.7 deg	210.6 km	3401 K	
9	13:52:23.4	51 km	turb	34.7 deg	199.1 km	3377 K	
10	13:52:28.4	45 km	turb	42.6 deg	166.1 km	3142 K	
11	13:52:37.6	38 km	turb	56.2 deg	133.1 km	2091 K	(no spectra)

Flow Field Simulation with DPLR

DPLR - Data-Parallel Line Relaxation code:

- 3-D nonequilibrium Navier-Stokes flow solver.
- includes the effects of finite-rate chemistry and thermal nonequilibrium
- Standard code used by NASA for high-speed flow computations.
- Validated over a wide spectrum of flight and ground-based experimental simulations.
- DPLR solves the equations for conservation of mass, momentum, and energy.
- Axisymmetric solutions converged to steady state with global time stepping.

Forebody block: 81 x 121
Aftbody block: 125 x 121

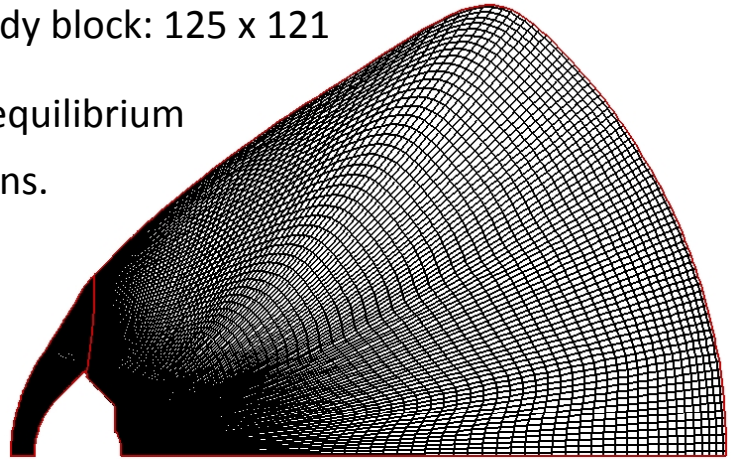

- Park's 1990 11-species air chemistry model includes N_2, O_2, NO, NO+, N_2+, O_2+, N, O, N+, O+, e
- Fully coupled finite rate chemistry was modeled with Park's 1990 curve fits.
- A two-temperature (T and T_v) model with the vibrational temperature in nonequilibrium was used.
- The surface was in radiative equilibrium with an emissivity value of 0.89 and fully catalytic.
- Solutions run fully laminar or fully turbulent (with Baldwin-Lomax turbulence model), with roughness induced transition predicted by Re_{kk}=100 predicted at 58km altitude for Hayabusa.
- For comparison purposes, both laminar and turbulent solutions generated for all altitudes.

Wright, M.W., White, T., and Mangini, N., "Data Parallel Line Relaxation (DPLR) Code User Manual Acadia – Version 4.01.1," NASA/TM-2009-215388, October 2009.

Material Response - FIAT

Fully Implicit Ablation and Thermal Response Program*

- 1-D time-accurate solution of thermal diffusion with surface ablation and internal pyrolysis
  - Similar equations to the Aerotherm CMA code but with greater stability
- Multilayer material stack
  - TPS, adhesive, insulation, structure, air gap, etc.
  - Planar, cylindrical, or spherical geometry
  - For Hayabusa carbon phenolic was used as TPS material

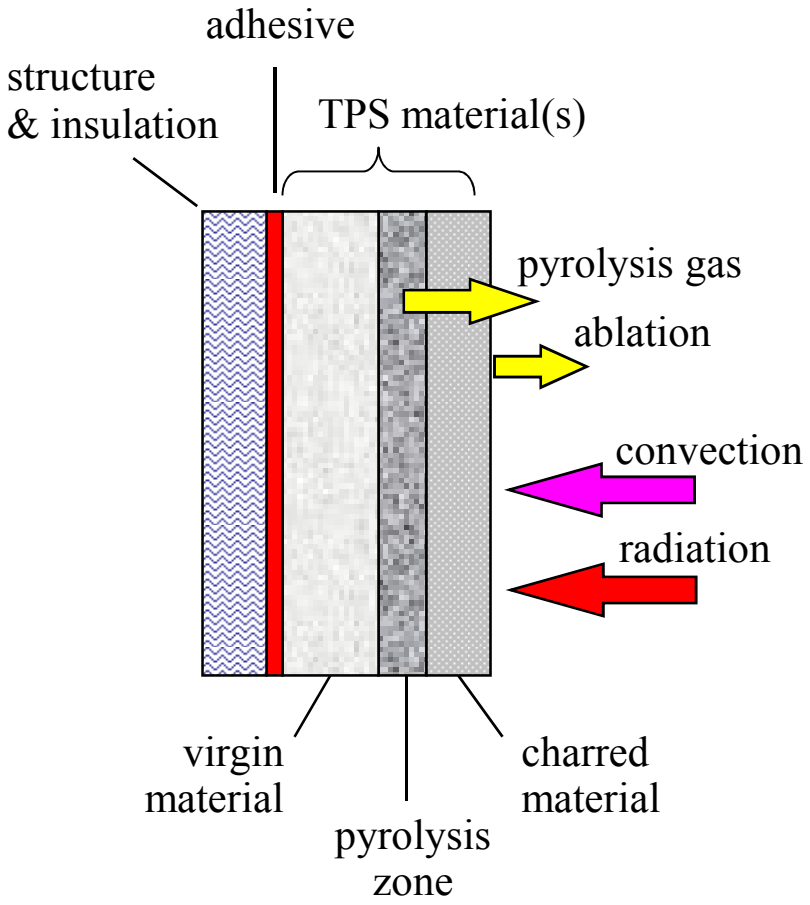

* Y.-K. Chen and F.S. Milos, "Ablation and Thermal Response Program for Spacecraft Heatshield Analysis," *Journal of Spacecraft and Rockets*, Vol. 36, No. 3, 1999, pp. 475-483.

§ C.B. Moyer and R.A. Rindal, "An Analysis of the Coupled Chemically Reacting Boundary Layer and Charring Ablator, Part II. Finite Difference Solution for the in-Depth Response of Charring Materials Considering Surface Chemical and Energy Balances," NASA CR-1061, 1968.

NEQAIR

- The Nonequilibrium Air Radiation (NEQAIR) code is a line-by-line radiation code that computes the emission and absorption spectra (along a line-of-sight) for atomic species, molecular species electronic band systems, and infrared band systems. Individual electronic transitions are evaluated for atomic and molecular species.
- The code can model the bound-free and free-free continuum radiation caused by interactions of electrons with neutral and ionized atomic species.
- Line broadenings due to Doppler, Stark, resonance, and collisional broadening as well as the natural line width are included in the code through Voigt broadening. Additional broadening (e.g. instrument broadening) can be included, in the form of both Lorentzian and Gaussian broadening.
- The radiative emission is computed along a line-of-sight. The line-of-sight is divided into a series of one-dimensional cells, and the radiative emission, absorption, and specific intensity are computed at every line-of-sight cell
- Radiative heating rate on a surface can be determined using either a tangent slab or spherical cap assumption.
- NEQAIR is capable of simulating the emission of a variety of species such as atoms (N, O, H, C, He) and molecules (N_2, N_2^+, NO, O_2, H_2, CO, C_2, CN).
However, for the present Haybusa analysis only O, N, N_2 and O_2 were used due to the wavelength range of concern and the available input from DPLR.

Radiation Transport

- Both plasma and surface radiation are computed in spectral radiance values i.e. power per emitting surface, wavelength interval and solid angle in the units W m^{-2} nm^{-1} sr^{-1} .
- Along the trajectory, the effective emitting surface will change due to the changing view angle and the solid angle will vary with the distance to the observer.
- Therefore, a calibration of the instruments to spectral radiance cannot be performed in a straightforward way and the emitted radiance has to be converted to spectral irradiance (received power per receiving surface in the units W m^{-2} nm^{-1})
- For this purpose, all computed spectral radiance values will be converted to a spectral radiant flux in W/nm by multiplying with the emitting surface and the solid angle in which radiation is emitted and then divided by the receiving surface given by the smallest aperture in the detection set-up. (The aperture diameter finally cancels out since it is used both for the solid angle and the receiving surface.)
- Needed quantities:
  distance Hayabusa-DC8, emitting surface area (grid cell for plasma, projected Hayabusa surface for thermal radiation), view angle.
- The same procedure was applied to the calibration sources.

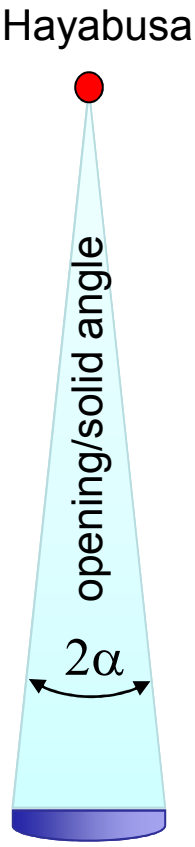

$$\Omega = 2\,\pi\,(1-\cos(\alpha))$$